5

The interior of Io

William B. Moore, Gerald Schubert, John D. Anderson, and John R. Spencer

Io is the Galilean satellite nearest to Jupiter and it is therefore subject to the most intense tidal forces. These forces deform Io in a way that is determined by the properties of Io's interior, thus, we can use measurements of the deformation of Io to obtain information on Io's internal structure. Io's rotational and tidal deformation was measured by imaging (Thomas *et al.*, 1998) and by Earth-based Doppler tracking of the *Galileo* spacecraft during several fly-bys of the satellite between 1999 and 2002 and during insertion of the spacecraft into Jupiter orbit in 1995 (Anderson *et al.*, 1996, 2001; Schubert *et al.*, 2004). Even prior to the *Galileo* spacecraft's observations of Io's tidal deformation, the moon's mass and radius and therefore density were known from *Pioneer* and *Voyager* spacecraft observations. The *Galileo* spacecraft data improved the accuracy of measurements of Io's mass and radius and determined Io's quadrupole gravitational coefficients.

Table 5.1 summarizes Io's basic physical properties. Io is about the size of the Earth's Moon, but it is considerably more dense (the lunar density is 3,341 $\mathrm{kg\,m^{-3}}$), indicating that there is more iron in Io than in the Moon. In fact, on the basis of density alone, it can be inferred that Io has an iron core of considerable size. Moreover, if the density is supplemented by shape information (the 3 ellipsoidal radii of the tidally and rotationally distorted Io) available from *Voyager* limb measurements, and it is assumed that Io is in hydrostatic equilibrium, the size of Io's iron core can be well constrained (Segatz *et al.*, 1988). So, even before the *Galileo* mission, we had a good idea about the basic structure of Io's interior. The *Galileo* measurements of the tidally and rotationally distorted Ionian gravitational field have verified the equilibrium shape of Io and have provided better constraints on interior models of the satellite. Below, we will show that Io is a two-layer body consisting of a metallic core and a silicate mantle. Io's intensive volcanic activity and crater-free surface also suggests it likely that the satellite has differentiated a global crustal layer below which lies a partially molten asthenosphere.

Table 5.1. Basic physical properties of Io (Schubert *et al.*, 2004).

Property	Value
Rotation rate, ω	4.1106×10^{-5} rad s^{-1}
Rotation period, $2\pi/\omega$	1.769 d
Orbital period	1.769 d
Radius, R	1,821.6 km
Mass, M	8.9319×10^{22} kg
Mean density	3,527.5 kg m^{-3}
Surface gravity, g	1.796 m s^{-2}
J_2	$1{,}859.5 \times 10^{-6}\, GM/R$
C_{22}	$558.8 \times 10^{-6}\, GM/R$
k_2	1.3043
q_r	1713.7×10^{-6}
$C/(MR^2)$	0.378

5.1 TIDAL AND ROTATIONAL DEFORMATION

Io is in synchronous rotation, meaning that its orbital period and rotational period are equal so that Io keeps one face to Jupiter at all times. Since Io is rotating, it experiences a centrifugal force that acts to flatten its shape. By keeping the same face to Jupiter, Io also experiences a steady tidal force that acts to elongate it along the line from Io to Jupiter. These forces are both nearly constant, since Io's rotation rate changes very slowly and its orientation toward Jupiter remains nearly fixed. Io has therefore had time to relax into an equilibrium shape which, to first order, is a triaxial ellipsoid, with the long axis pointing toward Jupiter and the short axis aligned with the rotation pole. In this section we show how the response of Io to tidal and rotational forces may be used to understand Io's interior.

The steady forcing potentials due to rotation and tides Φ_{2r} and Φ_{2t} are given by (Kaula, 1964):

$$\Phi_{2r} = \frac{\omega^2 r^2}{3}\left(P_{20}(\cos\theta) - 1\right) \tag{5.1}$$

$$\Phi_{2t} = -\frac{GM_J}{a}\left(\frac{r}{a}\right)P_{20}(\cos\alpha) \tag{5.2}$$

where ω is the rotational angular frequency, r is the radial distance from the center of the satellite, M_J is the mass of the primary (Jupiter), a is the semimajor axis of the satellite's orbit, θ is the colatitude measured from the north pole, and α is the angle from the line connecting the centers of the satellite and primary. The second term in brackets in (5.1) is spherically symmetric and does not contribute to the aspherical shape of Io, therefore we ignore it. The form of the tidal potential arises from a Taylor expansion of the gravitational potential of Jupiter in powers of r/a about the center of mass of Io, retaining only the r^2 term. The time-dependent parts of the tidal potential

depend on the eccentricity and lead to dynamic tides which drive the volcanic activity of Io as described below.

For a synchronously rotating satellite, Kepler's third law ($\omega^2 = GM_J/a^3$) and the trigonometric relationship $\cos\alpha = \sin\theta\cos\phi$ lead to the following time-independent potential Φ_2 at the surface of the satellite ($r = R$):

$$\Phi_2 = \Phi_{2t} + \Phi_{2r} = \omega^2 R^2 \left(-\frac{5}{6} P_{20}(\cos\theta) + \frac{1}{4} P_{22}(\cos\theta)\cos 2\phi \right) \tag{5.3}$$

where ϕ is the longitude about the rotation axis measured eastward from the sub-Jovian point.

The deformation of Io in response to the second degree potential given in (5.3) may be calculated by assuming a hydrostatic (or fluid) response. The billions of years over which these potentials have acted and the strong heating of Io evident in its volcanic activity should ensure that any stresses have been relaxed away by viscous deformation. The surface and internal density interfaces and iso-surfaces are therefore also equipotential surfaces, as required for hydrostatic balance.

The aspherical mass distribution arising from the deformation results in an additional deformation potential Φ_{2d}. The observed potential Φ is therefore the sum of the driving potential Φ_2 and the deformation potential Φ_{2d}. Since the deformation potential is linearly related to the driving potential, the observed potential may be generally expressed as:

$$\Phi = \frac{GM}{R}\left[-J_2 P_{20}(\cos\theta) + C_{22} P_{22}(\cos\theta)\cos 2\phi\right] \tag{5.4}$$

where J_2 and C_{22} are dimensionless potential coefficients. The linear relationship allows us to normalize the deformation potential by the driving potential, yielding the second-degree potential Love number k_2:

$$k_2 = \frac{\Phi_{2d}}{\Phi_2} = \frac{\Phi - \Phi_2}{\Phi_2} \tag{5.5}$$

It should be noted that the Love number will be a strong function of the forcing frequency for a viscoelastic body. The discussion here relates to the nearly zero-frequency (static) rotational and tidal potentials (5.3) and not to the semi-diurnal tides that are the result of Io's eccentricity and that give rise to its internal heating.

The value of k_2 for Io can be found by taking measurements of the gravitational field of Io to yield an estimate of Φ_{2d}, as suggested by Hubbard and Anderson (1978). Alternatively, the shape of Io can be measured from images of the limb to estimate the surface deformation directly. Both of these approaches have been applied to the data from the *Galileo* mission (Thomas *et al.*, 1998; Anderson *et al.*, 2001) and are reviewed in the next two sections.

5.2 IO'S GRAVITATIONAL FIELD

The gravitational field of Io was measured by Anderson *et al.* (2001) using Doppler tracking of the *Galileo* spacecraft as it flew by the satellite on four separate orbits. A

gravity field complete to degree and order three was solved for, but only the degree two components are significant. A combined solution for the degree-two components of Io's gravitational field was obtained yielding the dimensionless gravity field coefficients $J_2 = 1,846 \pm 4 \times 10^{-6}$ and $C_{22} = 554 \pm 1 \times 10^{-6}$. No significant S_{22} component (which would indicate a mis-alignment of the tidal bulge away from the line toward Jupiter) was found, nor were the asymmetric coefficients (e.g., C_{21}) different from zero. Thus, Io is deformed into a triaxial ellipsoid oriented toward Jupiter, as expected.

In order to improve the reliability of the solution, an a priori constraint that the observed coefficients J_2 and C_{22} would be in the 10/3 ratio as predicted by equations (5.3) and (5.4) was introduced. A solution without this constraint found similar values but suffered from large formal errors. Although in the literature this ratio is often used to show that a body is in hydrostatic equilibrium, the 10/3 ratio only demonstrates a linear response to the potential Φ_2. Departures from this ratio require mass anomalies with non-hydrostatic support, but the 10/3 value only indicates the absence of such mass anomalies, not the absence of, say, elastic stresses.

From the observed coefficients, we can construct an estimate of k_2. The C_{22} component is purely tidal, as can be seen from (5.1), making it simpler to write the ratio between the deformation potential (the observed C_{22} times GM/R) and the driving potential from (5.3) yielding:

$$k_2 = 4q_r C_{22} = 1.292 \pm 0.003 \tag{5.6}$$

where $q_r = \omega^2 R^3/GM$ is the ratio of the centrifugal and gravitational potentials at the equator. This value is significantly different from 1.5, the value for a homogeneous, fluid body, indicating a concentration of mass toward the center of Io that reduces the hydrostatic tidal response.

5.3 THE SHAPE OF IO

The aspherical deformation of Io may also be observed directly by analyzing images of the limb and fitting an ellipsoid. On a pixel by pixel basis, Thomas *et al.* (1998) solved for the position of the limb in 18 images obtained by the *Galileo* spacecraft, at resolutions from 5–20 km per pixel. The limb position is fit to within about 0.1 pixels.

The best-fit solutions for an arbitrary ellipsoid agreed well with solutions which were a priori constrained to have equilibrium ratios of the axes $(b-c)/(a-c) = 0.2459$ (including higher order corrections to the first-order value of 0.25), indicating that Io's aspherical shape is an equilibrium response to the potential given in (5.3). The principal axes of the best-fit ellipsoid are $a = 1,829.7 \pm 0.6$, $b = 1,819.2 \pm 0.5$, and $c = 1,815.8 \pm 0.4$ km.

Assuming that Io has an equilibrium shape, we can use the dimensions of the ellipsoid to derive an estimate of the surface deformation Love number h_2, defined as:

$$h_2 = \frac{u_r g}{\Phi_2} \tag{5.7}$$

where u_r is the amplitude of the degree-two radial deformation of the surface of the body, and g is the acceleration of gravity at the surface. We can estimate h_2 using the observed value of $(a - b) = 10.5 \pm 0.8$ km using the relationship (Dermott and Thomas, 1988):

$$h_2 = \frac{2}{3}\frac{(a-b)}{Rq} = 2.242 \pm 0.167 \tag{5.8}$$

For a hydrostatic body, $h_2 = k_2 + 1$, therefore the deformation observed by image analysis is consistent with that observed by Doppler tracking, though the gravitational measurements are considerably more precise.

5.4 IO'S INTERNAL DENSITY STRUCTURE

Having obtained estimates of k_2 and h_2, and confirmation that Io has an equilibrium shape, models of Io's interior density structure may be constructed to satisfy the Love numbers (which are not independent) and the total mass. With only two integral constraints, unique solutions are not possible, but families of likely solutions may be derived.

The mean density of Io is 3,528 kg m^{-3}, and silicate volcanism (as well as abundant sulfur) is observed at the surface (McEwen *et al.*, 1998). It is reasonable, then, to explore models of Io's interior consisting of an outer silicate layer and, possibly, a deep metallic core consisting of iron with some amount of sulfur. Nickel, which commonly occurs with iron, is a minor component of the core and is close enough in density to iron to make it indistinguishable for our purposes.

The maximum tidal deformation of a body is achieved for a homogeneous density fluid, where k_2 and h_2 reach maxima of 3/2 and 5/2 respectively. Io's observed k_2 Love number of 1.292 could be explained either by a density profile that increases toward the center, or by elastic stresses. Before pursuing differentiated models, we provide some results that arise from considering Io to be homogeneous in density but elastic. This will allow us to understand the limits the hydrostatic models place on the interior density structure. A homogeneous Io could exhibit a k_2 less than 3/2 only through elastic strength which resists the tidal and rotational forces throughout the billions of years over which these have been acting. As pointed out above, it is unlikely that such stresses have not relaxed over that time, but we pursue this model to see what limits can be placed on the mechanical behavior and internal density structure of Io.

The classical solution for a homogeneous elastic body was given by Love (1944) as:

$$k_2 = \frac{3}{2}\left(1 + \frac{19\mu}{2\rho g R}\right)^{-1} \tag{5.9}$$

where μ is the shear modulus of the material making up Io. We can use this relationship to derive an upper bound on the shear modulus $\mu < 2 \times 10^8$ Pa. This is considerably lower than values typical for solids ($10^{10} - 10^{11}$ Pa), indicating that Io's

interior cannot be entirely solid. If Io is not homogeneous, but instead has a dense core, this upper limit is reduced further.

Love numbers for differentiated bodies may be calculated using a method originally developed by Alterman *et al.* (1959) in which the deformations are decomposed into spherical harmonics and the resulting 6th-order system of differential equations describing the deformation is solved in a number of uniform property layers (Segatz *et al.*, 1998). For a simple, two-layer body, however, the Darwin–Radau relationship provides an approximate (though highly accurate for the densities involved in planetary materials) relationship between the hydrostatic Love numbers and the density distribution.

$$h_2 = k_2 + 1 = \frac{5}{1 + \left(\frac{5}{2} - \frac{15}{4}\gamma\right)^2} \tag{5.10}$$

where γ is the moment of inertia factor:

$$\gamma = \frac{C}{MR^2} = \frac{2}{5}\left[\frac{\rho_m}{\bar{\rho}} + \left(1 - \frac{\rho_m}{\bar{\rho}}\right)\left(\frac{r_c}{R}\right)^2\right] \tag{5.11}$$

where C is the maximum moment of inertia, ρ_m and $\bar{\rho}$ are the mantle and mean densities, respectively, and r_c is the core radius.

Figure 5.1 shows the core density (upper curves) and shell (mantle) density (lower curves) for the families of two-layer hydrostatic models that satisfy the observed k_2 and total mass for Io. The measurement uncertainty on k_2 is roughly the width of the solid lines. Also shown (dotted) are the densities of pure metallic iron, 8,000 kg m^{-3}, and iron–iron sulfide eutectic, 5,150 kg m^{-3} (Usselman, 1975) at pressures of $\sim$ 8 GPa, typical of Io's core.

The hydrostatic curves show that models with shell densities in the range of silicate rocks and core densities in the range for iron–iron sulfide mixtures have core radii between 0.37 and 0.52 of Io's radius. These models have silicate mantles with densities similar to the Earth's uppermost mantle or the bulk Moon (3,250–3,300 kg m^{-3}). Lower mantle densities require cores that are not metallic, but are mixtures of rock and metal.

We have shown above that the observations are consistent with an equilibrium shape for Io, but that does not exclude the possibility of elastic stress in, for example, a cold lithosphere. In order to alter the equilibrium shape of Io, this lithosphere would have to be frozen in when Io had a different shape, and it would have to maintain the stresses over billions of years. Since Io was most likely closer to Jupiter in the past, the frozen-in shape would actually be more distorted (less spherical) than the current forcing would dictate. Thus, the inferred structure would be less differentiated than the actual structure, causing the curves in Figure 5.1 to move away from the uniform density line. Although we consider it quite unlikely that Io's lithosphere is able to maintain such stresses over billions of years while magma courses through it to feed surface volcanism, elastic stresses would make our estimates of core size lower bounds.

In principle, elastic support could be constrained independently by the measured h_2, since it is only for hydrostatic models that h_2 is required to be $k_2 + 1$, but the

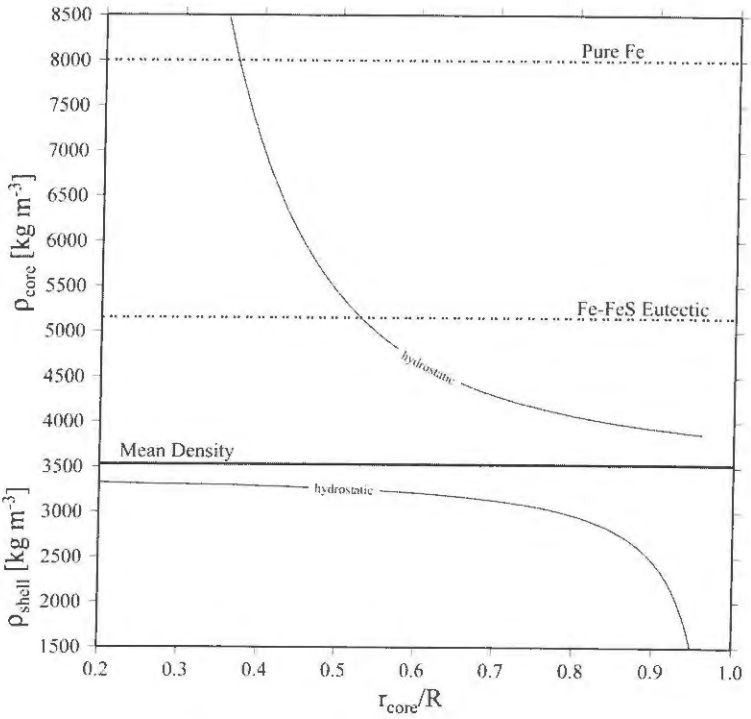

Figure 5.1. Two-layer models of Io consistent with the observed k_2 and mean density. The mean density is shown as a thick solid line dividing the core density curve (above) from the shell density curves (below). Also shown are the densities of pure Fe and the Fe–FeS eutectic.

measurement uncertainty on h_2 from the limb-fitting is too large to be helpful in this regard. A reduction in uncertainty by a factor of 2 in the h_2 measurement would allow this constraint to be used, at least for certain classes of models, to constrain the product of the lithospheric thickness and shear modulus.

Io's extensive volcanic activity suggests that the silicate mantle may be differentiated through the formation of a low-density crust (Keszthelyi and McEwen, 1997). We explore this possibility using three-layer models for the density structure (Anderson *et al.*, 2001). In order to reduce the degree of indeterminacy in the models, we restrict the core density to the end-member values for iron–iron sulfide mixtures. The results are not strongly sensitive to the assumed density of the crust for reasonable values between 2,500 and 3,000 kg m^{-3}, so we use an intermediate value appropriate to basalt of 2,750 kg m^{-3}. Figure 5.2 shows the resulting hydrostatic models that satisfy the observed k_2 and mean density as a function of crustal thickness.

The three-layer models show that a thick crust requires a dense mantle, which is not consistent with basaltic fractionation which removes iron from the mantle and leaves it less dense. If we restrict the mantle to densities near that of Earth's upper mantle (3,300 kg m^{-3}), then the crust must be less than about 40 km thick,

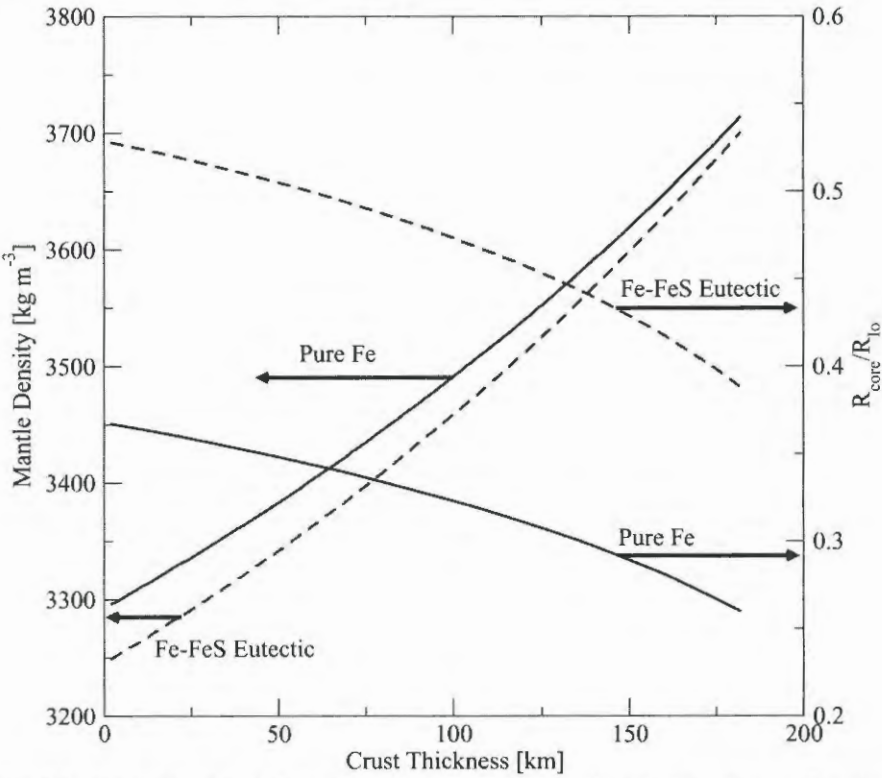

Figure 5.2. Mantle density (left axis) and fractional core radius (right axis) as a function of crustal thickness for the family of hydrostatic models satisfying the observed k_2 and mean density. The crustal density is 2,750 kg m^{-3}, and the range of core densities is most likely encompassed by the curves for pure Fe (solid) and the Fe–FeS eutectic (dashed).

independent of the density of the core. The radius of the core is mostly dependent on its density, ranging from about $0.35R_{Io}$ for a pure Fe composition to about $0.5R_{Io}$ for the Fe–FeS eutectic composition, for the same mantle density (3,300 kg m^{-3}).

Io may additionally have a partially molten asthenosphere, with a density intermediate between the differentiated crust and the unmelted mantle. With the constraints available, we cannot distinguish crust from asthenosphere and mantle. The smaller the density contrast between layers, the weaker the constraints on the layer thicknesses become. Such models are not inconsistent with the data, but the inherent indeterminacy makes them of little use.

5.5 THE COMPOSITION OF IO

Having determined the density structure of Io, we can now consider the chemical composition of Io and compare it to other Solar System bodies. The core of Io is 1/10

to 1/5 the total mass, depending on its composition, and the amount of iron in the core is 10–14% of the total. The Earth's core is nearly 1/4 its mass, the Moon's is less than 1/40 its mass, and the core of Mars is about 1/5 its mass. Mantle densities are restricted in a narrow range by the interior models (Figure 5.1), but mantle composition cannot be uniquely determined given the unknown temperature. Using the current equation of state data and assuming a pure olivine mantle, Sohl *et al.* (2002) derive mantle compositions between 76 and 85 wt% forsterite (Mg_2SiO_4) for super solidus mantles (temperatures between 1 and 1.2 times the solidus). The bulk Fe/Si ratios range from 1.3 to 1.5 for these models. Using a similar set of density models, Kuskov and Kronrod (2001) find that the L- and LL-chondrite meteorites are the best match for the composition of Io and derive a bulk Fe/Si ratio of 1.04 to 1.14. This value is very different from CI chondrites (1.71) (Kerridge and Matthews, 1988), the Moon (0.22-0.37) (Warren, 2005), or Mars (1.75–1.8) (Sohl *et al.*, 2005).

There is no real constraint on the composition of Io's core. Sulfur may be present at levels up to the eutectic (37 wt% FeS). Since the eutectic mixture would be the first to separate out, the core likely began eutectic but became more iron rich, as further heating would allow metallic iron to segregate. The amount of available metal depends critically on the oxidation state of Io's mantle and thus on that of the Jovian sub-nebula at Io's position. Hence, an independent measurement of the size of Io's core would provide a constraint on the redox conditions in the Jovian sub-nebula.

Io's composition seems to be consistent with the inference of orthopyroxene in surface magmas (Geissler *et al.*, 1999), since the L- and LL-chondrite compositions are pyroxene rich (Kuskov and Kronrod, 2001), although this was not accounted for in Sohl *et al.* (2002). The amount of iron in Io's mantle appears to be less than that in Mars, but considerably more than in the Moon or Earth. Io, then, appears to have condensed in an environment less oxidized than Mars, perhaps as a consequence of its formation in the Jovian sub-nebula.

5.6 IO'S SURFACE HEAT FLOW

An additional observation that can be brought to bear on the state of Io's interior is the heat flow at the surface. Unlike most bodies in the Solar System, which would require *in situ* methods to determine the heat flow, Io's surface heat flow can be estimated from remote observations of its thermal emission. Many discrete volcanic hot spots apparently account for most of the heat flow and their radiation is easily measured, but low-temperature emission from cooling lava flows may also be significant (Stevenson and McNamara, 1988; Veeder *et al.*, 1994), and is more difficult to separate from passive solar heating.

Disk-integrated, ground-based observations of Io's thermal emission provide uniform longitudinal coverage and a long time base, allowing study of the spatial

(longitudinal) and temporal variability of the heat flow. Veeder *et al.* (1994) constrained models of the passive component by wavelength-dependent changes in Io's thermal emission during Jupiter eclipses, by photometric observations of the bolometric albedo (Simonelli and Veverka, 1988) and *Voyager* infrared observations of Io's nightside temperature (Pearl and Sinton, 1982; McEwen *et al.*, 1996). They concluded that Io's average heat flow is more than 2.5 W m^{-2} (10^{14} W global total), with only modest temporal or spatial variability. They considered their estimate to be a lower limit because the ground-based data are not very sensitive to radiation from high-latitude anomalies, and because they did not include the possible contribution from heat conducted through Io's lithosphere.

Voyager infrared imaging spectrograph (IRIS) observations of Io (Pearl and Sinton, 1982; McEwen *et al.*, 1996) in the far infrared (5–50 μm), provide an independent measure of heat flow. The typical spatial resolution of these observations is a few hundred kilometers, which is sufficient to resolve individual hot spots. Relatively high spectral resolution allows some separation of passive and endogenic radiation within each field of view by fitting multiple black bodies to each spectrum and assuming that the lowest temperature contribution is passive. However, the data do not provide globally homogeneous coverage. Extrapolating from the Jupiter-facing hemisphere, where coverage is best, and assuming that Loki, which radiates more heat than any other Io hot spot (about 25% of the total), is unique, McEwen *et al.* (1996) estimated a minimum global heat flow of 1.85 W m^{-2}, with likely additional contributions from conducted heat and widespread low-temperature hot spots.

Endogenic emission is more readily separated from passive emission at night, when the passive component is minimized. *Voyager* IRIS obtained sporadic night-time coverage of Io, but the first hemispheric maps of broadband night-time emission came from *Galileo* photopolarimeter and radiometer (PPR) observations (Spencer *et al.*, 2000; Rathbun *et al.*, 2004). Low-latitude night-time temperatures away from the obvious hot spots are near 95 K, and drop more slowly than expected at high latitudes (e.g., 85 K at 70°S, 258°W). Making the assumption that at low latitudes the background temperature is entirely due to passive emission, and that all emission at higher temperatures is endogenic, Rathbun *et al.* (2004) estimated global heat flow to be 2 W m^{-2}, assuming that Loki is unique. The lack of fall-off in temperature with latitude would then imply excess endogenic emission at high latitudes. Rathbun *et al.* (2004) also determined that at low latitudes the diurnal surface temperatures away from the obvious hot spots was consistent with expected passive temperatures, given the bolometric albedo determined by Simonelli *et al.* (2001). Non-hot-spot endogenic emission, from conducted heat or widespread old cooling lava flows (Matson *et al.*, 2001) is therefore probably less than 1 W m^{-2}. From a global inventory of Io's thermal radiation from a variety of sources, McEwen *et al.* (2004) obtained a global heat flow estimate of 2.1 ± 0.7 W m^{-2}. The possibility of excess endogenic heat at high latitudes inferred from the warm night-time polar temperatures was incorporated into an updated version of their 1994 thermal model by Veeder *et al.* (2004) resulting in an estimated global heat flow of 3 ± 1 W m^{-2}. In summary, Io's total heat flow is still not precisely known, but all techniques give values in the range from 1.5–4 W m^{-2} ($0.6–1.6 \times 10^{14}$ W total).

5.7 THERMAL AND RHEOLOGICAL STRUCTURE

The tremendous heat flow measured at the surface of Io is the result of silicate volcanism, with typical inferred eruption temperatures of 1,200–1,400 K, and extreme temperatures over 1,800 K (McEwen *et al.*, 1998). It is likely that the sulfur-based volcanism observed by *Voyager* is also driven by silicate magma. Io is the most volcanically active body in the Solar System. The surface is so active that not a single impact crater has been identified in the images of the satellite. In this section we explore the implications of such activity for the thermal and rheological structure of the interior.

Despite the intensity of the volcanic activity on Io and the inferred high temperatures of its interior, Io supports some of the highest and steepest topography of any planetary body. Mountains up to 17 km high dot the surface (Jaeger *et al.*, 2003) and oddly, these are not volcanoes. Instead, volcanic centers are generally depressions, while the mountains appear to be fault-bounded tectonic uplifts. The presence of such large topography seems incompatible with a lithosphere that must allow the transport of $\sim 10^{14}$ W of heat.

A solution to this problem was found by O'Reilly and Davies (1981), who proposed a heat-pipe mechanism for heat transport through Io's lithosphere accomplished by melt transport through fissures. The most important implication of this model is that, as successive eruptions spread across the surface and cool, they bury the flows of previous eruptions, resulting in an advective transport of cold material from the surface downward.

In order to match the observed heat flow, Io must be resurfaced globally by silicate magma to a depth of 1–2 cm every year. This is then the rate at which material is advected downward within the lithosphere. The equation for the temperature T in the lithosphere is then:

$$\frac{k}{\rho c_P}\frac{d^2T}{dz^2} = v\frac{dT}{dz} - \frac{H}{\rho c_P} \tag{5.12}$$

where k is the thermal conductivity, ρ is the density, c_P is the specific heat, z is the depth from the surface, v is the downward velocity (resurfacing rate), and H is the volumetric heat production. The temperature must match the surface temperature T_s at the surface and the melting temperature T_m at the base of the lithosphere. The solution in the case of no heat production is:

$$T(z) = T_s + \frac{(T_m - T_s)(\exp^{\lambda\xi} - 1)}{\exp^{\lambda} - 1} \tag{5.13}$$

where $\xi = z/D$ is the depth normalized by the thickness of the lithosphere D, and the dimensionless parameter $\lambda = Dv\rho c_P/k$ is the advective velocity normalized by the conductive velocity scale. This can be related to the heat flux carried by melting F as follows:

$$\lambda = \frac{Dc_P F}{k\left[L_f + c_P(T_m - T_s)\right]} \tag{5.14}$$

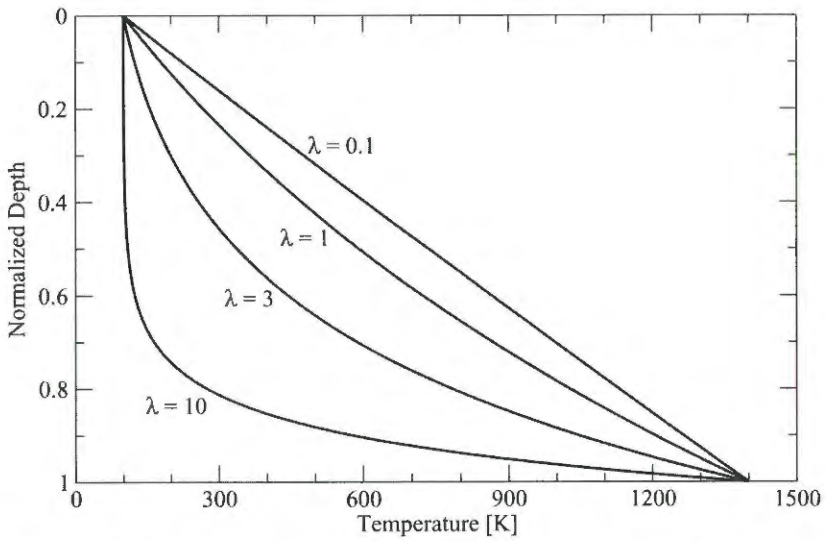

Figure 5.3. Temperature as a function of normalized depth for different values of λ, the normalized advective velocity defined in the text.

where L_f is the latent heat of fusion of the silicate rocks. For a heat flux of 2.5 W m^{-2} and a 30 km thick lithosphere, λ is about 10. Solutions for different values of λ are shown in Figure 5.3. For λ of 3, more than 80% of the thickness of the lithosphere is below 900 K, and for λ of 10, more than 95% of the lithosphere is cold enough to sustain elastic stresses for very long periods of time. This is how Io's lithosphere can support huge mountains while at the same time allowing a heat flux of 2.5 W m^{-2} to pass through.

The very steep gradient at the base of the lithosphere and the continuous flux of material through it means that any chemical layering in the lithosphere (i.e., crust) must be very closely linked to the rheological structure. That is, the crust and lithosphere are essentially the same. Schenk *et al.* (2001) pointed out that the lithosphere must be at least as thick as the tallest mountains (~15 km) if the mountains form as thrust blocks. In order to form the mountains by compressive stresses due to the global resurfacing, a thickness of at least 12 km is required (Jaeger *et al.*, 2003). As an upper limit, the tidal deformation will be restricted by a thick, strong lithosphere, so we can determine the maximum thickness elastic lithosphere (shear modulus 10^{11} Pa) that will allow Io to dissipate the observed heat flow. This limit turns out to not be very useful, since a 500-km elastic lithosphere is required to reduce the maximum dissipation below 10^{14} W.

What sort of melt fractions does the heat-pipe mechanism imply for the asthenosphere? It is straightforward to calculate the melt segregation velocity due to Darcy flow driven by the buoyancy of the melt (e.g., Scott and Stevenson, 1986):

$$\phi v = \frac{k_\phi g \Delta\rho}{\eta_m} \tag{5.15}$$

where ϕ is the melt volume fraction (porosity), g is the gravitational acceleration, $\Delta\rho$ is the difference between the solid and melt densities ($\sim$500 kg m^{-3}), η_m is the melt viscosity ($\sim$1,000 Pa s), and k_ϕ is the permeability, which is related to the porosity by a function of the form:

$$k_\phi = \frac{b^2\phi^n}{\tau} \tag{5.16}$$

where b is a typical grain size ($\sim$1 cm), and n and τ are constants which are functions of the geometry of the melt. The dependence of k_ϕ on grain size is overly simplified in this model, since real systems may have broad grain size distributions. Using the 1 cm yr^{-1} resurfacing velocity (which is actually the melt flux ϕv) and inserting experimentally determined values for the constants n (3) and τ (200) (Wark and Watson, 1998; Liang *et al.*, 2001) results in an estimate for ϕ between 10 and 20% (Moore, 2001). Melt fractions exceeding this will transport too much heat (the heat transported goes as k_ϕ), thus cooling the asthenosphere and bringing the melt fraction back to the equilibrium value.

Based on petrological models (using L- and LL-chondrite compositions, above), it has been pointed out by Keszthelyi *et al.* (1999, 2004) that the highest temperatures (up to 1,870 K) observed from surface eruptions on Io (McEwen *et al.*, 1998) require very bigh melt fractions (above 50%) in Io's interior. The apparent low viscosity of Ionian magmas also suggests ultramafic compositions and high melt fractions. Generalizing this to a global "mushy magma ocean" Keszthelyi *et al.* (2004) arrive at a model for Io's interior that is partially molten throughout, decreasing from 60% melt at the base of the lithosphere to 10–20% at the base of the mantle. Though attractive for its explanation of the very highest magma temperatures observed, it has not been shown how such a melt distribution can be maintained against melt segregation and the resulting heat loss (as described above), or bow such a rheological structure can allow sufficient tidal heat generation (Moore, 2001). The temperature of most eruptions observed on Io (1,200–1,400 K) seem to be consistent with the melt fractions (10–20%) required for thermal equilibrium (Moore, 2001), so perhaps there are local processes that account for the high-temperature outliers.

A rough estimate for the thickness of the asthenosphere may be obtained by extrapolating along the adiabat from the temperature at the top of the melt zone to the solidus:

$$d = \frac{\Delta T_m}{(dT/dz)_m - (dT/dz)_{ad}} \tag{5.17}$$

where $\Delta T_m = \phi L_f / c_P$ is the temperature excess required to reach a melt fraction ϕ, and the denominator is the difference between the slopes of the solidus ($\sim$ 0.8 K km^{-1}) and the adiabat ($\sim$ 0.1 K km^{-1}). Using the melt fractions estimated above, the asthenosphere is 60–120 km thick.

The physical state of Io's core cannot be determined from the *Galileo* spacecraft's observations of Io's permanent tidal deformation. The density difference between solid and liquid core material is too small to be resolvable from these data. If Io had a magnetic field, it would be possible to conclude that at least part of the core would have to be liquid. However, multiple fly-bys of Io by the *Galileo* spacecraft have shown

that Io does not possess an internal magnetic field (Kivelson *et al.*, 2004). All that can be concluded from the absence of a magnetic field is that there is insufficient convective activity in Io's core to support a dynamo. The core could be completely solid or liquid; it could even be partially solidified, although the lack of dynamo action would be more difficult to understand if there were a growing solid inner core in Io. Because Io's mantle is so intensely heated, it seems most likely that Io has no magnetic field because it has a completely liquid core that is kept from cooling and convecting by the surrounding hot mantle (Weinbruch and Spohn, 1995).

The state of the core is also not determined by the amount of tidal dissipation in Io, which is determined almost entirely by the viscosity of the mantle. Early work using parameterized (Q-model) dissipation (Peale *et al.*, 1979; Cassen *et al.*, 1982) suggested that a liquid core was required in order to allow the mantle to dissipate sufficient heat, but this is not supported by the results of more detailed calculations using the solutions to the equations of motion for viscoelastic bodies (Segatz *et al.*, 1988; Moore, 2003). The difference in dissipation between fluid cores and elastic cores in such models is less than a factor of 3.

5.8 THERMAL AND ORBITAL EVOLUTION

Io is unique in the Solar System in that its primary source of internal heat is not radioactive decay but tidal dissipation (Peale *et al.*, 1979). The tidal heat source is not only capable of much greater heating rates, it evolves with the orbit of Io, since it depends on both the distance of Io from Jupiter (the semi-major axis) and the eccentricity of Io's orbit. Tidal heating is also very sensitive to the rheology of Io's interior. The heat source is therefore coupled to both the orbit and the interior temperature. This results in a very different thermal evolution for Io than for other bodies of similar size (e.g., the Moon).

The tidal heating of Io's interior is a result of the resonant orbital interactions between Io, Europa, and Ganymede, which have orbital periods that are in the ratio $\tau_I:\tau_E:\tau_G = 1:2:4$. The orbits of all three satellites have evolved together into what is called the Laplace resonance, where the conjunctions of each satellite with its nearest outward neighbor occur when the inner satellite is at perijove (nearest to Jupiter) and the outer satellite at apojove (furthest from Jupiter), thus maximizing their separation. These repetitive alignments cause the orbits to remain elliptical, even though dissipation of tidal energy in the satellites should tend to circularize their orbits (while dissipation in Jupiter tends to make them more eccentric).

In addition to the effects of dissipation on eccentricity, tides raised on the satellite tend to reduce the semi-major axis of the orbit (i.e., the satellite tends to spiral inward). Thus, Io's orbital evolution is tightly coupled to the thermal evolution of its interior. Conversely, tides raised on Jupiter by the satellite cause the satellite to spiral outward (like the Moon). Thus, Io's actual rate of orbital migration represents a balance between dissipation in Io and dissipation in Jupiter. Indeed, this orbital migration is thought to be the process by which the resonant configuration is assembled (Yoder, 1979).

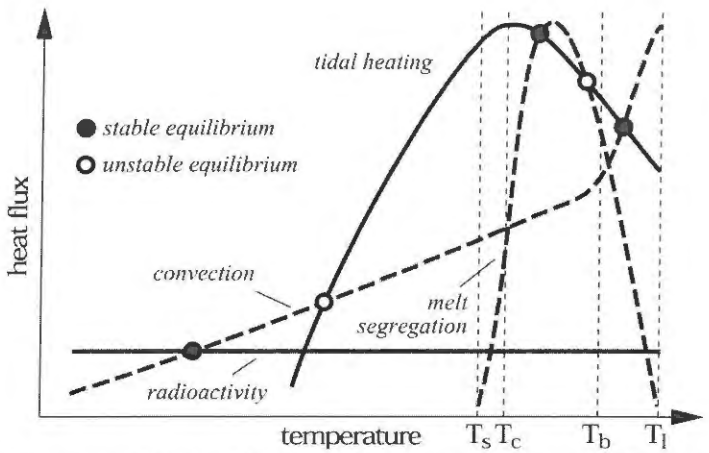

Figure 5.4. Depiction of the possible thermal equilibria (circles) in a tidally heated body. Heat sources (radioactivity and tidal heating) are shown as solid lines, and heat transport mechanisms (convection and melt segregation) are shown as dashed lines. Also marked schematically are the solidus T_s, critical T_c, breakdown T_b, and liquidus T_l temperatures.

The coupled thermal–orbital evolution of Io (and Europa and Ganymede) is a complex dynamical system with a wide possible range of behaviors. The interior temperature is set by the balance between tidal heating and heat transport (convective or magmatic). Orbital evolution is driven by dissipation in Io. Fischer and Spohn (1990) studied the coupled system including a simplified orbital evolution (linearized about the Laplace resonance) and convective heat transport, and recognized that there are multiple equilibria for the thermal state of Io, as illustrated in Figure 5.4, depicting the possible thermal equilibria in a tidally heated body. Radioactivity (solid line) produces the same heating regardless of temperature, while tidal heat production (solid curve) depends strongly on temperature, increasing with temperature until the Maxwell time (viscosity over shear modulus) of the material approaches the tidal forcing period. At a critical temperature (T_c) slightly above the solidus the shear modulus begins to decrease rapidly (Berckhemer *et al.*, 1982), resulting in a drop in tidal heating. At the breakdown temperature T_b, the solid matrix loses coherence, and the material becomes dominated by the mechanical properties of the liquid and the tidal heating is greatly reduced. Convective heat transport (dashed curve) increases with temperature, as the viscosity decreases, becoming extremely efficient as the liquidus temperature T_l is approached. Melt segregation (as described above) can only occur between the solidus and liquidus, and is not efficient above the breakdown temperature (since there is no longer any solid matrix for the melt to segregate from). Depending on the details of the heat production and transport processes, not all of these equilibria may be realized, so we use a qualitative diagram to illustrate the possible range of behaviors.

Fischer and Spohn (1990) identified the highest and lowest temperature equilibria (the points where the solid tidal heat and radioactivity curves intersect the dashed

convection curve) and noted that at times of low eccentricity, the high-temperature equilibrium may cease to exist. This is because low eccentricity shifts the tidal heat production curve downward, and it may fail to intersect the convective heat transport curve at all. Such episodes are followed by rapid cooling, as Io evolves toward the more common radioactivity driven convective equilibrium. Conversely, extremely high eccentricity could cause the low-temperature equilibrium to vanish, resulting in runaway heating toward the high-temperature equilibrium. Moore (2003) investigated the tidal–convective equilibrium (for the current eccentricity, independent of the orbital evolution) and concluded that the high-temperature equilibrium, while present, cannot explain the observed heat flow, thus a different heat transport process (melt segregation) was necessary.

Melt segregation can introduce additional equilibria as shown in Figure 5.4. These equilibria are necessarily between the solidus and liquidus temperatures (T_s and T_l). The simplified calculation given in Section 5.7 required melt fractions of 10–20% to achieve equilibrium. This equilibrium is stable, but may disappear at times of low eccentricity. Since this equilibrium is reached at temperatures lower than the convective equilibrium (this is a consequence of the high viscosity of rocks, even when partially molten), it is likely that Io never reaches the high-temperature convective equilibrium. Io's volcanic activity and high heat flow strongly suggest that Io is in (or near) an equilibrium state with melt segregation balancing tidal heat production.

It is not known whether our roughly three decades of heat flow observations are representative of the long-term average, but if 10^{14} W is the rate of energy dissipation in Io, then if we know the rate of dissipation in Jupiter, we can predict the rate at which Io's orbit is evolving. Unfortunately, the mechanisms by which tidal motions are dissipated in a deep atmosphere such as Jupiter's are not understood at present. We are therefore left with trying to measure the orbital evolution to estimate dissipation in Jupiter.

Recent attempts to measure the rate of Io's orbit migration using astrometric measurements of satellite mutual events (eclipses) disagree on both the rate and the direction of the orbital migration. The process used to infer the migration rate of Io from the mutual event timing is apparently quite model dependent, since Lieske (1987) derives a rate of change of the mean motion of Io $\dot{n}/n$ of $-0.74 \pm 0.87 \times 10^{-11}$ yr^{-1}, while a more recent measurement using a different orbital theory by Aksnes and Franklin (2001) yields a rate of $+36 \pm 10 \times 10^{-11}$ yr^{-1}.

We can put certain bounds on the total outward migration of Io's orbit (assuming Europa and Ganymede have moved in concert) by assuming Io formed as close to Jupiter as possible (2.4 R_J) and evolved to its current orbital distance over the age of the Solar System. This upper bound on the migration rate, however, is still much too low to account for Io's current dissipation rate, which depends on the maintenance of a high eccentricity (and thus high dissipation in Jupiter) (Yoder and Peale, 1981). We are therefore forced to conclude that Io's orbital evolution has not been steady over the age of the Solar System, or that the current heat flow does not represent a long-term average of the tidal dissipation.

Either case is possible, since we do not know if the Laplace resonance is primordial or if it was assembled more recently by orbital migration. Furthermore, Io's

surface heat flow represents dissipation integrated over some unknown transport time. However, if most of the heat is carried by melt segregation, as seems to be the case (above and Moore, 2003) the transport time is short (tens of years), and the heat flow does reflect recent tidal dissipation. A longer transport time regulated by convective motions would allow for the possibility of oscillatory states in which the heat flow and dissipation are out of phase (Fischer and Spohn, 1990; Hussmann and Spohn, 2004).

5.9 SUMMARY

The *Galileo* mission to Jupiter has greatly advanced our understanding of Io. It is now clear that Io is a differentiated body consisting of a metallic core and a silicate mantle. The radius of the core is between 0.37 and 0.52 times Io's radius, depending on the unknown composition. The composition of the mantle is also not known precisely, but the best analogy to Io's composition are the L- and LL-chondrite meteorites. The bulk Fe–Si ratio is well below CI chondrites and Mars, but higher than the Moon. The physical state of the core is unknown, but it is likely liquid (due to the intensely heated mantle above). Though a differentiated crust of some sort is inevitable, we cannot constrain its thickness or composition.

The strong lithosphere required to support the observed mountains is a consequence of the large flux of molten rock to the surface, which rapidly buries older, cold flows. This melt segregation is responsible for nearly all of Io's very high surface heat flux, and most likely drives the sulfur volcanism that makes Io's surface so distinctive. Melt fractions in the mantle required to balance the observed heat flow are 10–20%, which is consistent with the bulk of the temperature estimates for surface flows, though there may be localized regions at higher temperature with higher melt fractions.

Since Io's heat flow is dominated by the relatively rapid process of melt segregation, the available heat flow data are most likely representative of the average heat production by tidal dissipation in Io's interior. Though measurements of the orbital evolution of Io are at present inconclusive, future measurements (e.g., from an orbiter) should establish its rate of migration and constrain the dissipation in Jupiter.

5.10 REFERENCES

Aksnes, K. and F. A. Franklin. 2001. Secular acceleration of Io derived from mutual satellite events. *Astronomical Journal*, **122**(5), 2734–2739.

Alterman, Z., H. Jarosch, and C. L. Pekeris. 1959. Oscillations of the Earth. *Proc. R. Soc. London Ser. A.*, **252**, 80–95.

Anderson, J. D., W. L. Sjogren, and G. Schubert. 1996. Galileo gravity results and the internal structure of Io. *Science*, **272**, 709–712.

Anderson, J. D., R. A. Jacobson, E. L. Lau, W. B. Moore, and G. Schubert. 2001. Io's gravity field and interior structure. *J. Geophys. Res.*, **106**, 32963–32969.

Berckhemer, H., W. Kampfmann, E. Aulbach, and H. Schmeling. 1982. Shear modulus and Q of forsterite and dunite near partial melting from forced-oscillation experiments. *Phys. Earth Planet. Int.*, **29**, 30–41.

Cassen, P. M., S. J. Peale, and R. T. Reynolds. 1982. Structure and evolution of the Galilean satellites. In: D. Morrison and M. S. Matthews (eds), *Satellites of Jupiter*. University of Arizona Press, Tucson, AZ, pp. 93–128.

Dermott, S. F. and P. C. Thomas. 1988. The shape and internal structure of Mimas. *Icarus*, **73**, 25–65.

Fischer, H. J. and T. Spohn. 1990. Thermal–orbital histories of viscoelastic models of Io (J1). *Icarus*, **83**, 39–65.

Geissler, P. E., A. S. McEwen, L. Keszthelyi, R. Lopes-Gautier, J. Granahan, and D. P. Simonelli. 1999. Global color variations on Io. *Icarus*, **140**(2), 265–282.

Hubbard, W. B. and J. D. Anderson. 1978. Possible flyby measurements of Galilean satellite interior structure. *Icarus*, **33**, 336–341.

Hussmann, H. and T. Spohn. 2004. Thermal–orbital evolution of Io and Europa. *Icarus*, **171**(2), 391–410.

Jaeger, W. L., E. P. Turtle, L. P. Keszthelyi, J. Radebaugh, and A. S. McEwen. 2003. Orogenic tectonism on Io. *Journal of Geophys. Res.*, **108**(E8), doi:10.1029/2002JE001946.

Kaula, W. M. 1964. Tidal dissipation by solid friction and the resulting orbital evolution. *Rev. Geophys.*, **2**, 661–685.

Kerridge, J. F. and M. S. Matthews. 1988. *Meteorites and the Early Solar System*. University of Arizona Press, Tucson, AZ.

Keszthelyi, L. and A. McEwen. 1997. Magmatic differentiation of Io. *Icarus*, **130**, 437–448.

Keszthelyi, L., A. S. McEwen, and G. J. Taylor. 1999. Revisiting the hypothesis of a mushy global magma ocean in Io. *Icarus*, **141**, 415–419.

Keszthelyi, L., W. L. Jaeger, E. P. Turtle, M. Milazzo, and J. Radebaugh. 2004. A post-Galileo view of Io's interior. *Icarus*, **169**(1), 271–286.

Kivelson, M. G., F. Bagenal, W. S. Kurth, F. M. Neubauer, C. Paranicas, and J. Saur. 2004. Magnetospheric interactions with satellites. In: F. Bagenal, T. E. Dowling, and W. B. McKinnon (eds), *Jupiter: The Planet, Satellites and Magnetosphere*. Cambridge University Press, Cambridge, UK, pp. 513–536.

Kuskov, O. L. and V. A. Kronrod. 2001. Core sizes and internal structure of the Earth's and Jupiter's satellites. *Icarus*, **151**, 204–227.

Liang, Y., J. D. Price, D. A. Wark, and E. B. Watson. 2001. Nonlinear pressure diffusion in a porous medium: Approximate solutions with applications to permeability measurements using transient pulse decay method. *Journal of Geophys. Res.*, **106**, 529–535.

Lieske, J. H. 1987. Galilean satellite evolution: Observational evidence for secular changes in mean motions. *Astron. Astrophys.*, **176**, 146–158.

Love, A. E. H. 1944. *A Treatise on the Mathematical Theory of Elasticity*. Dover, New York.

Matson, D. L., T. V. Johnson, G. J. Veeder, D. L. Blaney, and A. G. Davies. 2001. Upper bound on Io's heat flow. *Journal of Geophys. Res.*, **106**(E12), 33021–33024.

McEwen, A. S., Keszthelyi, L. P., Spencer, J. R., Schubert, G., Matson, D. L., Lopes-Gautier, R., Klaasen, K. P., Johnson, T. V., Head, J. W., Geissler, P. *et al.* 1998. High-temperature silicate volcanism on Jupiter's moon Io. *Science*, **281**(5373), 87–90.

McEwen, A. S., N. R. Isbell, K. E. Edwards, and J. C. Pearl. 1996. Temperatures on Io: Implications to geophysics, volcanology, and volatile transport. *Lun. Planet. Inst. Conf. Abs.*, **27**, 843.

McEwen, A. S., L. P. Keszthelyi, R. Lopes, P. M. Schenk, and J. R. Spencer. 2004. The lithosphere and surface of Io. In: F. Bagenal, T. E. Dowling, and W. B. McKinnon

(eds), *Jupiter: The Planet, Satellites and Magnetosphere*. Cambridge University Press, Cambridge, UK, pp. 307–328.

Moore, W. B. 2001. The thermal state of Io. *Icarus*, **154**, 548–550.

Moore, W. B. 2003. Tidal heating and convection in Io. *Journal of Geophys. Res.*, **108**, 5096, doi:10.1029/2002JE001943.

O'Reilly, T. C. and G. F. Davies. 1981. Magma transport of heat on Io: A mechanism allowing a thick lithosphere. *Geophys. Res. Lett.*, **8**, 313–316.

Peale, S. J., P. Cassen, and R. T. Reynolds. 1979. Melting of Io by tidal dissipation. *Science*, **203**, 892–894.

Pearl, J. C. and W. M. Sinton. 1982. Hot spots of Io. In: D. Morrison and M. S. Matthews (eds), *Satellites of Jupiter*. University of Arizona Press, Tucson, AZ, pp. 724–755.

Rathbun, J. A., J. R. Spencer, L. K. Tamppari, T. Z. Martin, L. Barnard, and L. D. Travis. 2004. Mapping of Io's thermal radiation by the Galileo photopolarimeter–radiometer (PPR) instrument. *Icarus*, **169**(1), 127–139.

Schenk, P., H. Hargitai, R. Wilson, A. McEwen, and P. Thomas. 2001. The mountains of Io: Global and geological perspectives from Voyager and Galileo. *Journal of Geophys. Res.*, [in press].

Schubert, G., J. D. Anderson, T. Spohn, and W. B. McKinnon. 2004. Interior composition, structure and dynamics of the Galilean satellites. In: F. Bagenal, T. E. Dowling, and W. B. McKinnon (eds), *Jupiter: The Planet, Satellites and Magnetosphere*. Cambridge University Press, Cambridge, UK, pp. 281–306.

Scott, D. R. and D. J. Stevenson. 1986. Magma ascent by porous flow. *Journal of Geophys. Res.*, **91**, 9283–9296.

Segatz, M., T. Spohn, M. N. Ross, and G. Schubert. 1988. Tidal dissipation, surface heat flow, and figure of viscoelastic models of Io. *Icarus*, **75**, 187–206.

Simonelli, D. P. and J. Veverka. 1988. Bolometric albedos and diurnal temperatures of the brightest regions on Io. *Icarus*, **74**(2), 240–261.

Simonelli, D. P., C. Dodd, and J. Veverka. 2001. Regolith variations on Io: Implications for bolometric albedos. *Journal of Geophys. Res.*, **106**(E12), 33241–33252.

Sohl, F., T. Spohn, D. Breuer, and K. Nagel. 2002. Implications from Galileo observations on the interior structure and chemistry of the Galilean satellites. *Icarus*, **157**(1), 104–119.

Sohl, F., G. Schubert, and T. Spohn. 2005. Geophysical constraints on the composition and structure of the Martian interior. *Journal of Geophys. Res.*, [in press].

Spencer, J., J. Rathbun, L. Travis, L. Tamppari, L. Barnard, T. Martin, and A. McEwen. 2000. Io's thermal emission from the Galileo photopolarimeter–radiometer. *Science*, **288**(5469), 1198–1201.

Stevenson, D. J. and S. C. McNamara. 1988. Background heatflow on hotspot planets – Io and Venus. *Geophys. Res. Lett.*, **15**(13), 1455–1458.

Thomas, P., *et al.* 1998. The shape of Io from Galileo limb measurements. *Icarus*, **135**(1), 175–180.

Usselman, T. M. 1975. Experimental approach to the state of the core. *American Journal of Science*, **275**, 291–303.

Veeder, G. J., D. L. Matson, T. V. Johnson, D. L. Blaney, and J. D. Gougen. 1994. Io's heat flow from infrared radiometry: 1983–1993. *J. Geophys. Res.*, **99**, 17095–17162.

Veeder, G. J., D. L. Matson, T. V. Johnson, A. G. Davies, and D. L. Blaney. 2004. The polar contribution to the heat flow of Io. *Icarus*, **169**(1), 264–270.

Wark, D. A. and E. B. Watson. 1998. Grain-scale permeabilities of texturally equilibrated, monomineralic rocks. *Earth Planet. Sci. Lett.*, **164**, 591–605.

Warren, P. H., "New" lunar meteorites: Implications for composition of the global lunar surface, lunar crust, and the bulk Moon. *Meteoritics & Planet. Sci.*, **40**(3), 477–506.

Wienbruch, U. and T. Spohn. 1995. A self-sustained magnetic field on Io? *Planetary and Space Science*, **43**, 1045–1057.

Yoder, C. F. 1979. How tidal heating in Io drives the Galilean orbital resonance locks. *Nature*, **279**, 767–770.

Yoder, C. F. and S. J. Peale. 1981. The tides of Io. *Icarus*, **47**, 1–35.